



PCCP

**Spectroscopic Evidence for Intact Carbonic Acid Stabilized  
by Halide Anions in the Gas Phase**

Journal:	<i>Physical Chemistry Chemical Physics</i>
Manuscript ID	CP-ART-04-2020-002338.R1
Article Type:	Paper
Date Submitted by the Author:	09-Jun-2020
Complete List of Authors:	Zhang, Hanhui; University of Science and Technology of China Cao, Wenjin; Pacific Northwest National Laboratory Yuan, Qinqin; Pacific Northwest National Laboratory Wang, Lei; University of Science and Technology of China Zhou, Xiaoguo; University of Science and Technology of China Liu, Shilin; University of Science and Technology of China Wang, Xue-Bin; Pacific Northwest National Laboratory

SCHOLARONE™  
Manuscripts

## ARTICLE

## Spectroscopic Evidence for Intact Carbonic Acid Stabilized by Halide Anions in the Gas Phase

Received 00th January 20xx,  
Accepted 00th January 20xx

DOI: 10.1039/x0xx00000x

Hanhui Zhang,<sup>a</sup> Wenjin Cao,<sup>b</sup> Qinqin Yuan,<sup>b</sup> Lei Wang,<sup>a</sup> Xiaoguo Zhou,<sup>\*a</sup> Shilin Liu,<sup>a</sup> and Xue-Bin Wang<sup>\*b</sup>

This work shows elusive carbonic acid being effectively stabilized in the gas phase by interacting with halide anions  $X^-$  ( $X = F, Cl, Br, \text{ and } I$ ). The formed  $H_2CO_3 \cdot X^-$  complexes, characterized by negative ion photoelectron spectroscopy and *ab initio* calculations, all contain intact *trans-trans* carbonic acid binding onto the respective halide via two identical strong ionic  $O-H \cdots X^-$  hydrogen bonds. For  $X = Cl, Br, \text{ and } I$ , the complex spectra exhibit the corresponding  $X^-$  signature by simply shifting to higher binding energy side, while an extremely broader band of 2 eV range is observed for  $X = F$ . These spectroscopic evidences indicate that the excess electron is removed from each halide in the former case, while a proton is transferred from carbonic acid to fluoride upon electron detachment for the latter. The above  $H_2CO_3 \cdot X^-$  structures as well as those of the previously studied  $H_2SO_4 \cdot X^-$  along the homologous halogen series cannot be explained using the proton affinity (PA) argument. Instead, a qualitative correlation is found between those structural motifs and the constituent acid *pKa* values, strongly suggesting that *pKa* is a more suitable factor to predict correct acid-base chemistry between these diprotic oxyacids and halides.

### Introduction

Carbonic acid is a diprotic oxyacid of fundamental interest in geography,<sup>1,2</sup> astrophysics,<sup>3-5</sup> biochemistry<sup>6,7</sup> and other related fields. It not only contributes to ocean acidification and affects the organic matter and nutrients,<sup>1</sup> but it also serves as a prospective interstellar molecule on the Martian surface, comets and icy grains.<sup>3-5</sup> Moreover, it plays vital physiological roles in the  $H_2CO_3/HCO_3^-$  buffer system that stabilizes the blood *pH* and other biological fluids,<sup>6</sup> maintaining a large flux of protons that sustain metabolic life-supporting processes and rapid enzymatic reactions.<sup>7</sup> Therefore, the molecular conformation of carbonic acid-containing complexes, especially those involving strong hydrogen bonding, is crucial to understanding its related chemical reactivities.

For a long time, carbonic acid has generally been considered to be thermodynamically unstable, undergoing dissociation to carbon dioxide and water in gas phase. Although a potential well was suggested by theoretical calculations for the isolated carbonic acid,<sup>8</sup>

the catalyzations by various ambient species, like solvents, surfaces or other constituents in solution, can efficiently lower the barrier.<sup>9-11</sup> In 1987, Schwarz and coworkers performed the first direct detection of gas-phase  $H_2CO_3$  molecule in mass spectra of the heated ammonium bicarbonate ( $NH_4HCO_3$ ) vapor.<sup>12</sup> The first spectroscopic measurement was done in 2009 using Fourier-transform microwave spectroscopy, in which the gaseous *cis-trans*  $H_2CO_3$  molecule was produced by passing a pulsed electric discharge of carbon dioxide in supersonic expansion conditions through a water reservoir.<sup>13</sup> In addition, a debate has proceeded for more than 20 years on the two polymorphs of solid carbonic acid,  $\alpha$ - and  $\beta$ - $H_2CO_3$ .<sup>14-21</sup> Despite a lot of spectral characterization reported for both of them,<sup>22-24</sup> Reisenauer et.al. verified that  $\alpha$ - $H_2CO_3$  actually belongs to carbonic acid monomethyl ester, while the  $\beta$  polymorph is true  $H_2CO_3$ .<sup>25</sup>

Compared with its gas and solid phases, the aqueous carbonic acid is relatively more complicated. The deuterated carbonic acid yielded by ultrafast protonation of bicarbonate in deuterium oxide solution was reported to have a limited lifetime of 300 nanoseconds.<sup>26</sup> Such a fleeting lifetime implies that hydrogen bonding interaction between carbonic acid and Lewis bases like water might be central to its related chemical processes instead of carbonic acid itself. A recent investigation<sup>7</sup> also confirmed that in spite of its instability, carbonic acid could still serve as an effective protonating agent by matching its *pKa* value, which has been accurately determined over the full physiological temperature range, perfectly accounting for its vital biological function. Despite some progresses have been made, there is a lack in investigations about the interactions between carbonic acid and more Lewis bases beyond the water. Of particular interest are anions of high Lewis

<sup>a</sup> Hefei National Laboratory for Physical Sciences at the Microscale, Department of Chemical Physics, University of Science and Technology of China, Hefei, Anhui 230026, P. R. China. Email: xzhou@ustc.edu.cn

<sup>b</sup> Physical Sciences Division, Pacific Northwest National Laboratory, 902 Battelle Boulevard, P. O. Box 999, MS K8-88, Richland, Washington 99352, USA. Email: xuebin.wang@pnnl.gov

\*Electronic Supplementary Information (ESI) available: [Optimized structures of the *trans-trans* neutral radicals (Figure S1), Electron density topological graphs (Figure S2), NPA charge distributions (Figure S3), Schematic structures of all isomers of  $H_2CO_3 \cdot F^-$  and their neutrals (Figure S4), Frank-Condon simulated spectra for different isomers of  $H_2CO_3 \cdot F^-$  (Figure S5), Binding energies of carbonic acid and halides (Table S1), Topological properties of  $H_2CO_3 \cdot X^-$  (Table S2), and Relative energies and enthalpies of formation of  $H_2CO_3 \cdot X^-$  in Isomer 1 conformation (Table S3)]. See DOI: 10.1039/x0xx00000x

basicity such as halide anions, whose hydrogen bonding structures between carbonic acid and the ligands can provide detailed insights into the stabilization and chemistry of carbonic acid in solutions. Very recently, Thomas *et al.* measured the infrared action spectrum of carbonic acid-fluoride complex anion in helium nanodroplets.<sup>27</sup> A strong ionic double hydrogen bond was proved to be the core for the remarkable stability of  $F^-(H_2CO_3)$  with carbonic acid in a *trans-trans* conformation. Unfortunately, no other halide complex anions were observed in their experiments, preventing a systematic understanding of halide induced stabilization of carbonic acid over the whole series.

Notably, the fluoride anion always formed distinct hydrogen bonds than the other halides because it has the smallest ionic radius and highest Lewis basicity, which leads to unique local solvation structures in protic solvents, such as  $F^-(H_2O)_2$ <sup>28, 29</sup> and  $H_2SO_4 \cdot F^-$ .<sup>30</sup> Although proton affinity (PA) is usually thought as the determinant factor for a hydrogen bonding structure between proton donor and acceptor, this criterion fails in  $H_2SO_4 \cdot X^-$  ( $X = Cl, Br, I$ )<sup>30</sup> and a few other molecular clusters.<sup>31-36</sup> Thus, a comprehensive investigation of all halide- $H_2CO_3$  complexes is necessary to find the true determinant factor for hydrogen bonding structures at a molecular level, since the PA values span a wide range in the F, Cl, Br, I sequence. In addition, the halides-water and halides-carbon dioxide complexes have been investigated,<sup>28, 37-38</sup> as well as the  $HCO_3^-$  dissolved in water molecule clusters,<sup>39</sup> providing requisite fundamental knowledge for in-depth understanding of carbonic acid-halide interactions.

## Experimental and theoretical methodologies

**Negative ion photoelectron spectroscopy (NIPES).** The NIPES spectra were recorded using the low-temperature, magnetic-bottle time-of-flight (TOF) photoelectron spectrometer, coupled with an electrospray ionization source and a temperature-controlled cryogenic ion trap.<sup>40</sup> The  $H_2CO_3 \cdot F^-$  complex anions were produced by electrospraying a  $\sim 0.1 \times 10^{-3}$  M mixture solution of NaF salt in water/acetonitrile (1/3 ratio) under an environment containing a relatively high concentration of carbon dioxide vapor. The generation of the other halide clusters was slightly different: aqueous solutions of  $KX$  ( $X = Cl, Br, I$ ) salt with a concentration of  $\sim 0.4 \times 10^{-3}$  M were bubbled by a flow of carbon dioxide for 30 minutes, and then mixed into acetonitrile at a volume ratio of 1:3. The carbonic acid-halide anions were generated by electrospraying the solutions into vacuum, while the sample cone was exposed to a  $CO_2$  flow passing through a bubbler of water.

All produced anions were guided by two RF-only quadruples into a 3D cryogenic ion trap, where they were accumulated and cooled down at  $\sim 20$  K. The cold anions were then pulsed out into the extraction zone of the TOF mass spectrometer at 10 Hz, and the desired anions were mass-selected, decelerated, and intercepted by a probe laser beam in the photodetachment zone of the magnetic-bottle photoelectron analyzer. In the current experiment, a 157 nm  $F_2$  laser and a 193 nm ArF excimer laser were used to detach electrons from target complex anions containing fluoride and the other halides, respectively. The lasers were operated at a 20 Hz repetition rate with the anion beam turned off at alternating laser shots, enabling shot-by-shot background subtraction. Using a 5.2 m-

long magnetic-bottle electron flight tube, the TOF distribution of the detached electrons was analyzed, and then converted into a kinetic energy spectrum after calibration with the known data of  $I^-$ ,  $Cu(CN)_2^-$  and  $Au(CN)_2^-$ . The electron binding energies (eBEs) of anions were determined by subtracting the electron kinetic energies from the photon energies used.

**Theoretical methods.** To study the structures, energetics, and spectral features of the complex anions  $H_2CO_3 \cdot X^-$  ( $X = F, Cl, Br, \text{ and } I$ ) and their corresponding neutrals, CCSD(T) calculations were performed. The aug-cc-pVTZ-PP basis set with the Stuttgart-Köln MCDHF RSC ECP (10 and 28 core electrons respectively)<sup>41</sup> was used for Br and I atoms, while the standard all-electron aug-cc-pVTZ basis set<sup>42</sup> was adopted for all other atoms. Both basis sets were obtained from the EMSL Basis Set Exchange.<sup>43, 44</sup> All geometry optimizations were conducted without any initial symmetry constraints, and vibrational frequency analyses were carried out to ensure the true minima being obtained and to calculate the zero-point energy (ZPE) corrections. For comparison, the multi-reference configuration interaction (MRCI) calculations were also performed for each  $H_2CO_3 \cdot X^-$  ( $X = Cl, Br, \text{ and } I$ ) anion and the corresponding neutral molecule using the optimized geometries obtained at the CCSD(T) or the CASSCF(6,8) (for anion) and CASSCF(5,8) (for neutral) levels, respectively. Such active spaces were chosen to include all the halogen  $np$  electrons among the eight valence orbitals (three  $p$  orbitals for halogen, two unoccupied  $p$  orbitals for carbon, and three unoccupied  $p$  orbitals for three oxygens).

For the complex anions, the vertical detachment energy (VDE) was calculated as the energy difference between the neutral and the corresponding anion, both at the optimized anion's geometry, while the adiabatic detachment energy (ADE) was determined as the energy difference between the neutral and anion, each at its own optimized geometry including ZPE corrections. In addition, to assess the spin-orbit (SO) coupling effect for open-shell neutral radicals, the Breit-Pauli operator,<sup>45, 46</sup> together with the third-order Douglas-Kroll-Hess scalar relativistic corrections<sup>47</sup> for the  $X = Br$  and  $I$  complexes, was used in the MRCI calculations with a slightly difference basis set, i.e., the aug-cc-pVTZ-DK of the Douglas-Kroll contracted basis set<sup>48</sup> for Br/I atoms and aug-cc-pVTZ basis set for all other atoms. All the CCSD(T) and MRCI calculations were performed using the MOLPRO 2015.1 software package.<sup>49</sup>

## Results and discussion

### NIPES spectra

In this work, NIPES combined with electrospray ionization source is applied, a methodology which has been proved as a powerful experimental technique to probe molecular structures of complex clusters.<sup>50-52</sup> Many hard efforts were made to challenge the difficulties in generation of all carbonic acid-halide complexes in order to render a comprehensive comparison of all  $H_2CO_3 \cdot X^-$  ( $X = F, Cl, Br, \text{ and } I$ ) NIPES spectra. Figure 1 shows the low-temperature NIPES spectra of  $H_2CO_3 \cdot X^-$  ( $X = Cl, Br, \text{ and } I$ ) photodetached at 193 nm (6.424 eV) and  $H_2CO_3 \cdot F^-$  at 157 nm (7.867 eV). Compared to isolated halide anions, all complex anions have significantly higher electron binding energies (eBEs), indicating that the extra electron is substantially stabilized by  $H_2CO_3$  in the clusters. The NIPES

spectrum of  $\text{H}_2\text{CO}_3\cdot\text{I}^-$  contains two dominant peaks centered at 4.10

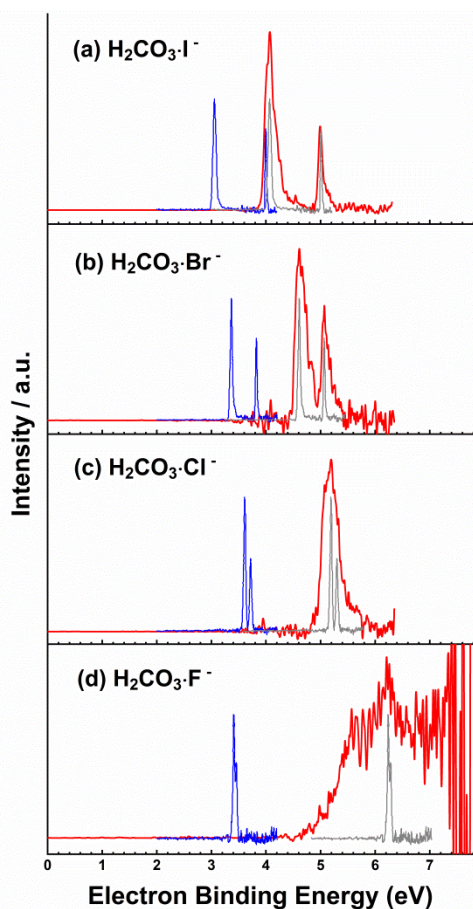


**Figure 1.** Low-temperature photoelectron spectra of  $\text{H}_2\text{CO}_3\cdot\text{X}^-$  ( $\text{X}=\text{Cl}$ ,  $\text{Br}$ , and  $\text{I}$ ) at 193 nm (6.424 eV) and  $\text{H}_2\text{CO}_3\cdot\text{F}^-$  at 157 nm (7.867 eV). The blue and gray curves are the original and shifted spectra of the corresponding isolated halides, respectively, which are adapted from Ref. 53.

and 5.02 eV, respectively. Because of the 0.92 eV energy interval, which is close to the SO splitting of iodine (0.943 eV)<sup>53</sup>, the two bands are easily designated to the contributions of  $\text{H}_2\text{CO}_3\cdot\text{I}(^2P_{3/2})$  and  $\text{H}_2\text{CO}_3\cdot\text{I}(^2P_{1/2})$ . Compared to the NIPE spectrum of isolated iodide anion (the blue curve in Figure 1a), each SO splitting peak is broadened presumably due to vibrational excitations accompanied in the photodetachment process. Moreover, the lower eBE band of  $\text{H}_2\text{CO}_3\cdot\text{I}(^2P_{3/2})$  is wider in details than the  $\text{H}_2\text{CO}_3\cdot\text{I}(^2P_{1/2})$  band at the higher eBE side. This disparity can be attributed to the further splitting of  $\text{I}(^2P_{3/2})$  state due to electrostatic interaction with the close-shell  $\text{H}_2\text{CO}_3$  at sufficiently a small distance. In Hund's case (a), the  $^2P_{3/2}$  state can split into  $X(1/2)$  and  $A(3/2)$  sub-states which is determined by the projection ( $\Omega$ ) of the total electronic angular momentum onto the symmetry axis.<sup>37-38, 54</sup> However, no splitting occurs for the  $^2P_{1/2}$  state, leaving the  $B(1/2)$  in a unique state.

Similarly, two distinct peaks were located at 4.61 and 5.07 eV for  $\text{H}_2\text{CO}_3\cdot\text{Br}^-$  complex anion, and the 0.46 eV energy gap is also identical to the SO splitting of 0.457 eV for  $\text{Br}(^2P_{3/2}$  and  $^2P_{1/2})$ .<sup>53</sup> In the case of  $\text{H}_2\text{CO}_3\cdot\text{Cl}^-$  complex anion, only one unresolved wide peak was observed with the center at 5.20 eV, due to too small SO splitting of  $\text{Cl}$  (0.109 eV)<sup>53</sup>. Thus, the consistent assignments are

obtained for these three  $\text{H}_2\text{CO}_3\cdot\text{X}^-$  ( $\text{X}=\text{Cl}$ ,  $\text{Br}$ , and  $\text{I}$ ) complexes, that their NIPE spectra have identical patterns to those of the corresponding isolated halide anions with significant blue-shifts in eBEs. This observation strongly suggests that the electron is detached from the halide in complexes. In other words, the negative charge of the complexes remains in the halide moiety, and no proton transfer occurs during the formation of  $\text{H}_2\text{CO}_3\cdot\text{X}^-$  ( $\text{X}=\text{Cl}$ ,  $\text{Br}$ , and  $\text{I}$ ). The above conjecture appears consistent with the fact that the PA values of  $\text{X}^-$  (1395, 1353, and 1315 kJ/mol for  $\text{Cl}^-$ ,  $\text{Br}^-$ , and  $\text{I}^-$ , respectively<sup>55</sup>) are smaller than that of bicarbonate ( $\text{HCO}_3^-$ , 1490 kJ/mol),<sup>56</sup> thus hindering proton transfer (PT) from carbonic acid to the halide in the formation of the complex anions, as indicated by the NIPE spectra.

Taking the experimental resolution into account, the vertical detachment energies (VDEs) and the adiabatic detachment energies (ADEs) of the complex anions can be determined from the first peak maximum and onset threshold in the NIPE spectra. Table 1 summarizes the experimental VDEs and ADEs of  $\text{H}_2\text{CO}_3\cdot\text{X}^-$  ( $\text{X}=\text{Cl}$ ,  $\text{Br}$ , and  $\text{I}$ ), as well as the observable SO splittings. Their close VDE and ADE values for each complex imply that both geometries of neutral and anion are similar. Moreover, the eBE difference ( $\Delta\text{eBE}$ ) between the complex anions and the corresponding isolated anions directly reflects the interaction strength between the host neutral molecule and guest anion.<sup>57</sup> Since the apparently different widths exist for the complexes and the isolated halides,  $\Delta\text{VDEs}$  are more reliable to exhibit the binding energies between  $\text{H}_2\text{CO}_3$  and  $\text{X}^-$ , e.g. 1.58 eV for  $\text{H}_2\text{CO}_3\cdot\text{Cl}^-$ , 1.25 eV for  $\text{H}_2\text{CO}_3\cdot\text{Br}^-$ , and 1.04 eV for  $\text{H}_2\text{CO}_3\cdot\text{I}^-$ , respectively. Along the atomic sequence of  $\text{X}^-$  ( $\text{X}=\text{Cl}$ ,  $\text{Br}$ , and  $\text{I}$ ), the decreasing  $\Delta\text{VDE}$  value indicates a gradually reduced interaction strength between halide anion and  $\text{H}_2\text{CO}_3$ , which shows a consistent trend with the respective halide PAs.

In contrast to the  $\text{X}=\text{Cl}$ ,  $\text{Br}$  and  $\text{I}$  cases, the spectrum of  $\text{H}_2\text{CO}_3\cdot\text{F}^-$  in Figure 1d is markedly different from that of the isolated  $\text{F}^-$ . An extremely broadened band was observed, spanning the eBE range from 4.5 to 7.6 eV. The whole band can be roughly viewed as being consisted of partially resolved sub-bands, centered at ~5.5, 6.2 and ~6.9 eV, respectively. In the region near the photon energy limit at 157 nm, notable oscillations blurred the spectral profile to some extent due to the poor detection efficiency of low kinetic energy electrons and imperfect background subtraction. Apparently, the extraordinarily broadened band of  $\text{H}_2\text{CO}_3\cdot\text{F}^-$  cannot be attributed to the SO splitting of fluorine as was in the other  $\text{H}_2\text{CO}_3\cdot\text{X}^-$  anions, implying that  $\text{H}_2\text{CO}_3\cdot\text{F}^-$  might have different molecular structure from the others. Because  $\text{F}^-$  has a larger PA (1556 kJ/mol<sup>55</sup>) than  $\text{HCO}_3^-$  (1490 kJ/mol<sup>56</sup>), it is entirely reasonable to assume an intramolecular PT during the complex formation that produces the  $[\text{HOC}(\text{O})\text{O}\cdots\text{HF}]$  structure. The complex anion of  $[\text{HOC}(\text{O})\text{O}\cdots\text{HF}]$  deservedly has a similar spectral motif to  $\text{HCO}_3^-$ ,<sup>58, 59</sup> however, their experimental spectra are entirely inconsistent. Therefore, high-level quantum chemical calculations and spectral analysis are needed to help illuminate the true origins of the spectral complexity for  $\text{H}_2\text{CO}_3\cdot\text{F}^-$  (see next sections). In addition, the VDE of 6.24 eV and ADE of 4.72 eV, derived from the spectrum yields a 2.5 eV  $|\text{VDE} - \text{ADE}|$  difference for  $\text{H}_2\text{CO}_3\cdot\text{F}^-$ , a difference much larger than other  $\text{H}_2\text{CO}_3\cdot\text{X}^-$  ( $\text{X}=\text{Cl}$ ,  $\text{Br}$ , and  $\text{I}$ ) complexes, indicative of demonstrable changes regarding its molecular geometry during electron detachment. The obtained

$\Delta$ VDE of 2.82 eV blueshift from isolated  $F^-$  is also the largest among all four complexes.

**Table 1.** Theoretical and experimental ADEs, VDEs, and binding energies (BEs) for the  $H_2CO_3 \cdot X^-$  ( $X = F, Cl, Br, \text{ and } I$ ) complex anions, as well as the spin-orbit (SO) splittings of the photodetached neutral complexes and isolated halogens.

X	ADE (eV)			VDE (eV)			BE (eV)		SO Splitting(eV)	
	Expt.	CCSD(T)	MRCI	Expt.	CCSD(T)	MRCI	Expt. <sup>a</sup>	CCSD(T)	Expt. <sup>b</sup>	MRCI
F	4.72	4.60	---	6.24	6.13	---	2.82	2.63	---(0.051)	---
Cl	4.96	5.33	5.16	5.2	5.67	5.61	1.58	1.56	---(0.109)	0.22
Br	4.52	4.94	4.49	4.61	5.17	4.83	1.25	1.35	0.46(0.457)	0.48
I	3.99	4.50	4.07	4.10	4.65	4.31	1.04	1.12	0.92(0.943)	1.04

<sup>a</sup>The experimental binding energy (BE) is determined as  $\Delta$ VDE from the isolated halide anions. <sup>b</sup>The experimental SO splitting for complex anions is determined as the energy difference between the  $^2P_{3/2}$  and  $^2P_{1/2}$  states. The values in the parentheses are the SO splitting values of halogen atoms from the spectra of the isolated halides (from Ref. 53).

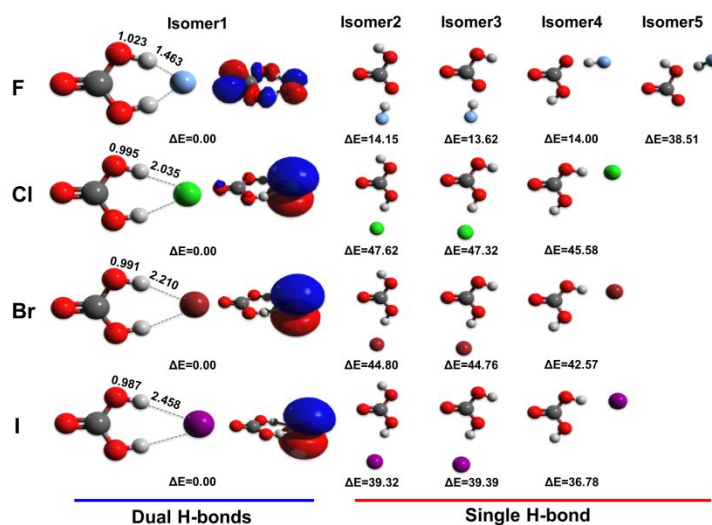


**Fig. 2** Optimized geometries and related energies (in kJ/mol) of isomers for  $H_2CO_3 \cdot X^-$  ( $X = F, Cl, Br, \text{ and } I$ ) complex anions, calculated at CCSD(T)/aug-cc-pVTZ(-PP) level of theory, where the distances of O-H and H...X bonds are noted with the unit of Å. The highest occupied molecular orbitals (HOMOs) of Isomer1 are exhibited as well.

### Optimized structures and energetics

It is well-known that  $H_2CO_3$  has three conformers, namely *cis-cis*, *cis-trans*, *trans-trans*, suggesting that PT may occur along different geometries with the approach of  $X^-$ . Thus, both the reactant and product of PT with  $[HOC(O)OH \cdots X^-]$  and  $[HOC(O)O^- \cdots HX]$  structures were initially assumed and checked in geometry optimizations. To our surprise, they eventually converged to a unique optimized one for each type. Moreover, like another diprotic oxyacid of  $H_2SO_4 \cdot X^-$ ,<sup>30</sup> the complex anions with double hydrogen bonds might also be formed with *trans-trans*  $H_2CO_3$ , as reported in the previous IR action spectroscopy of  $H_2CO_3 \cdot F^-$ .<sup>27</sup> In this study we successfully obtained the optimized geometries for multiple  $H_2CO_3 \cdot X^-$  anion isomers at the CCSD(T) level, as shown in Figure 2. In general, these isomers can be classified into two families, *i.e.*, one with formation of double hydrogen bonds (Isomer1), and the others with single hydrogen bond (Isomers 2–5). The calculated relative energies of all complex anion isomers after the zero-point energy (ZPE) corrections are also listed in Figure 2.

For the single hydrogen-bond structures of  $H_2CO_3 \cdot X^-$  ( $X = Cl, Br, \text{ and } I$ ), Isomers 2, 3 and 4 are formed when  $X^-$  approaches the *cis-cis*, *cis-trans*, *trans-cis*  $H_2CO_3$  conformers, respectively. These isomers are of  $[HOC(O)OH \cdots X^-]$  ( $X = Cl, Br, I$ ) structure as shown in Figure 2, while the  $[HOC(O)O^- \cdots HF]$  is predicted for  $H_2CO_3 \cdot F^-$  isomers. This change is consistent with the PA sequence of the constituent anions, where  $I^- < Br^- < Cl^- < HCO_3^- < F^-$ . Due to the fact that isomers 2, 3, 4 differ only in the conformer of  $H_2CO_3$  ( $X = Cl, Br, I$ ) ( $HCO_3$  for  $X = F$ ) and all belong to the binding motif with a single hydrogen-bond, all the isomers have close energies and the geometry of the  $H_2CO_3$  moiety remains intact for the large halide complexes. Of special interest is the observation that the energy sequence of these  $H_2CO_3$  conformers in the complexes is different from those of isolated carbonic acid. At the CCSD(T) level, the *cis-cis* conformer is most stable for carbonic acid itself, while the *cis-trans* and *trans-trans* conformers have higher energies of 6.53 and 40.25 kJ/mol, respectively. However, under the action of  $X^-$  ( $X = Cl, Br, \text{ and } I$ ), Isomer 4 in the *cis-trans* conformation is slightly more stable compared to the others (Isomers 2 and 3) owing to the reduced repulsive force between  $X^-$  and carbonyl oxygen. Notably, a special

Isomer 5 was found for  $\text{H}_2\text{CO}_3\cdot\text{F}^-$  complex, in which the formed HF molecule is connected to the remaining hydroxyl. Evidently, this isomer can be produced by the subsequent HF migration of Isomer 4, when  $\text{F}^-$  approaches the *trans*-OH group. That is, the formed HF group of Isomer 4 can further migrate to the other side to produce the  $[\text{O}_2\text{COH}\cdots\text{HF}]$  structure. However, as indicated in Figure 2, this migration is endothermic by  $\sim 24$  kJ/mol from Isomer 4.

In Isomer 1, the carbonic acid moiety adopts the  $C_{2v}$  structure with a planar *trans-trans* conformation, and two hydrogen bonds are simultaneously formed between two hydroxyl groups and the halide anion, producing a loose six-membered ring structure (Figure 2). Isomer 1 is the most stable among all anion complex conformers, irrespective of different halide anion types, implying that the strong stabilization by dual hydrogen bonds makes the *trans-trans* conformation become the global minimum. Meanwhile, the double hydrogen bond provides an explanation for the significantly higher eBEs observed in experiments. Our present calculations are consistent with the recent study of  $\text{H}_2\text{CO}_3\cdot\text{F}^-$  by Thomas et al.<sup>27</sup> As shown in Figure 2, all geometries of Isomer 1 for  $\text{H}_2\text{CO}_3\cdot\text{X}^-$  are very similar, in which both hydroxyl hydrogen atoms remain in the carbonic acid without PT. Taking  $\text{H}_2\text{CO}_3\cdot\text{Cl}^-$  for instance, both O–H bond lengths are slightly increased from 0.963 Å in isolated carbonic acid to 0.995 Å, while the distance between chloride and hydroxyl hydrogen atom is 2.035 Å, a typical strong ionic hydrogen bond length of  $[\text{O}\cdots\text{H}\cdots\text{Cl}^-]$ . Moreover, along the sequence of  $\text{F}^- \rightarrow \text{Cl}^- \rightarrow \text{Br}^- \rightarrow \text{I}^-$ , the gradually shortened O–H bond length and elongated  $\text{X}\cdots\text{H}$  distance in the complexes are consistent with the charge-induced intensities of  $\text{X}^-$  indicated by their PA values.

It is worth noting that, for the  $\text{X} = \text{F}$  case, the  $\text{H}\cdots\text{F}$  distance is only 1.463 Å, a significantly shorter length than in the other cases. This strongly implies that two formed H–F bonds in this six-membered ring show evident covalent characteristics. These properties are hypothesized to be essential in causing its different spectral pattern in Figure 1d from that of isolated  $\text{F}^-$  or the other  $\text{H}_2\text{CO}_3\cdot\text{X}^-$  ( $\text{X} = \text{Cl}, \text{Br}, \text{and I}$ ) complexes. In addition, Isomers 2–4 of  $\text{H}_2\text{CO}_3\cdot\text{X}^-$  ( $\text{X} = \text{Cl}, \text{Br}, \text{and I}$ ) are higher than Isomer 1 by  $\sim 40$  kJ/mol. These energy differences are close to the isolated single hydrogen bond energy of  $\text{O}\cdots\text{H}\cdots\text{X}$ , indicating no significant repulsive interaction between the two hydrogen bonds in Isomer 1. In contrast, Isomers 2–4 of  $\text{H}_2\text{CO}_3\cdot\text{F}^-$  with a single hydrogen bond are only higher than Isomer 1 by  $\sim 14$  kJ/mol. This can be explained considering the shorter  $\text{H}\cdots\text{F}$  distances in Isomer 1 such that the repulsive interaction between two 2p orbitals of fluorine anion naturally enhances tension of the six-membered ring and reduces its stability. Based on the relative energies of these isomers of  $\text{H}_2\text{CO}_3\cdot\text{X}^-$ , only Isomer 1 is discussed in the following sections according to its dominant thermal distribution.

Using the optimized geometries of Isomer 1 and its associated optimized neutrals (Figure S1), the VDEs and ADEs of  $\text{H}_2\text{CO}_3\cdot\text{X}^-$  complex anions were calculated at both CCSD(T) and MRCI levels. The SO splitting of the corresponding neutral complex was also calculated at the MRCI level. As indicated in Table 1, a good agreement between the experimental and the calculated data at both CCSD(T) and MRCI levels of theory are achieved. Moreover, the binding energies (BEs) between  $\text{H}_2\text{CO}_3$  and halide in  $\text{H}_2\text{CO}_3\cdot\text{X}^-$

can be calculated according to equation (1) including ZPE corrections.

$$\text{BE} = E(\text{H}_2\text{CO}_3) + E(\text{X}^-) - E(\text{H}_2\text{CO}_3\cdot\text{X}^-) \quad (1)$$

where  $E(\text{H}_2\text{CO}_3)$ ,  $E(\text{X}^-)$  and  $E(\text{H}_2\text{CO}_3\cdot\text{X}^-)$  are the energies of neutral  $\text{H}_2\text{CO}_3$ , isolated  $\text{X}^-$  anion, and complex anion, each at its own optimized geometries with the same conformation. For the  $\text{H}_2\text{CO}_3\cdot\text{X}^-$  complex anions, the calculated BEs were 2.63, 1.56, 1.35, and 1.12 eV for  $\text{X} = \text{F}, \text{Cl}, \text{Br}, \text{and I}$ , respectively, as listed in Table S1. The variation trend of BEs agrees very well with the experimental  $\Delta\text{VDE}$  values.

### Bonding analyses and spectral simulations

As two representative diprotic oxyacids,  $\text{H}_2\text{CO}_3$  and  $\text{H}_2\text{SO}_4$  might have similar complex structures with halide anions. A recent investigation<sup>30</sup>, however revealed an unordinary structure of  $[\text{HSO}_4\cdots\text{HF}]$  for the sulfuric acid-fluoride complex, in which one  $\text{O}\cdots\text{H}\cdots\text{F}$  and one  $\text{O}\cdots\text{H}\cdots\text{F}$  hydrogen bond are formed with the approach of  $\text{F}^-$ , in contrast to  $[\text{H}_2\text{CO}_3\cdot\text{F}^-]$ , where the fluoride anion plays the role of acceptor for two identical  $\text{O}\cdots\text{H}\cdots\text{F}$  hydrogen bonds (Figure 2). Certain covalent bond characteristics were suggested for these  $\text{H}\cdots\text{F}$  bonds in  $[\text{H}_2\text{CO}_3\cdot\text{F}^-]$  to account for their short bond lengths. In order to quantify the chemical interactions along the whole series of  $[\text{H}_2\text{CO}_3\cdot\text{X}^-]$ , we further characterized their binding motifs with the electron density,  $\rho(r)$ , and charge populations for the  $\text{O}\cdots\text{H}\cdots\text{X}$  bonds of Isomer 1, using the theory of "atoms in molecules (AIM)"<sup>60, 61</sup> with the Multiwfn program<sup>62</sup> (Figure S2). On the electron localization function<sup>63</sup> surfaces of all  $\text{H}_2\text{CO}_3\cdot\text{X}^-$ , electrons along both  $\text{O}\cdots\text{H}\cdots\text{X}$  paths are predominantly localized between oxygen and hydrogen atoms, indicative of its covalent characteristics. Meanwhile, the covalent O–H bond strength increases in the sequence of  $\text{F} \rightarrow \text{Cl} \rightarrow \text{Br} \rightarrow \text{I}$  (Table S2), where the  $\text{X}^-$  anions play a charge inducer role. Moreover, natural population analyses (NPA) confirmed that more than 80% of the extra negative charge resides on halides in this complex anion series (Figure S3). The smooth bond strength change and similar NPA charges for all  $\text{H}_2\text{CO}_3\cdot\text{X}^-$  complex anions discussed above, nevertheless, appear to contradict the fact that an extraordinarily complicated spectrum is observed for  $\text{H}_2\text{CO}_3\cdot\text{X}^-$   $\text{X} = \text{F}$ , as compared to the simple spectra for  $\text{X} = \text{Cl}, \text{Br}, \text{and I}$ .

Since the highest occupied molecular orbital (HOMO) locates the primarily detached electron of complex anions, Figure 2 displays the calculated HOMOs of the Isomer 1 of  $\text{H}_2\text{CO}_3\cdot\text{X}^-$ . For  $\text{H}_2\text{CO}_3\cdot\text{X}^-$  ( $\text{X} = \text{Cl}, \text{Br}, \text{and I}$ ), the HOMO is mainly contributed by the  $p$  orbital of  $\text{X}^-$ , thus rendering these complex anions to exhibit similar photoelectron spectra of their respective isolated halides. However, to our surprise, the HOMO of  $\text{H}_2\text{CO}_3\cdot\text{F}^-$  is entirely different from the other carbonic acid-halide anions, even though the four complex anions look similar in the structural binding motif. As shown in Figure 2, the HOMO is primarily localized on the carbonyl oxygen of  $\text{H}_2\text{CO}_3\cdot\text{F}^-$ , while  $\text{F}^-$  also makes a significant contribution. Therefore, the NIPE spectrum of this complex anion should have a different pattern from that of isolated  $\text{F}^-$ .

As discussed above, the NIPE spectra of  $\text{H}_2\text{CO}_3\cdot\text{X}^-$  ( $\text{X} = \text{Cl}, \text{Br}, \text{and I}$ ) show similar spectral patterns to those of isolated halides, dominantly contributed from two SO states with the lower eBE band  $\text{X}(^2P_{3/2})$  further splitting into two sub-states of  $\text{X}(1/2)$  and  $\text{A}(3/2)$ ,<sup>37-38, 54</sup> while the  $^2P_{1/2}$  state remaining as the unique  $\text{B}(1/2)$



state. Thus, a simple spectral simulation of density of states (DOS) based on the theoretically generalized Koopman's theorem<sup>64, 65</sup> was applied to analyze the NIPE spectra of  $\text{H}_2\text{CO}_3\cdot\text{X}^-$  ( $\text{X} = \text{Cl}, \text{Br}, \text{and I}$ ). In

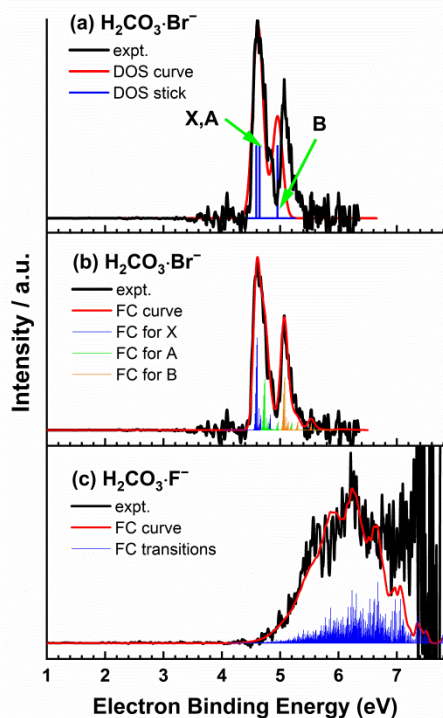


**Fig. 3** The density of state (DOS) (a), Franck-Condon (FC) factor simulated spectra of  $\text{H}_2\text{CO}_3\cdot\text{Br}^-$  (b), and  $\text{H}_2\text{CO}_3\cdot\text{F}^-$  (c) with  $\text{H}_2\text{CO}_3$  in *trans-trans* conformation. The corresponding experimental spectra are also exhibited for comparison.

addition, the Franck-Condon (FC) factor calculations were also performed using the ezSpectrum program<sup>66</sup> to simulate the accompanied vibrational structures in the spectra. To facilitate the comparisons, Figure 3 stands as an example to show the experimental, DOS and FC factor simulated spectra of  $\text{H}_2\text{CO}_3\cdot\text{Br}^-$  based on Isomer 1.

Apparently, major spectral patterns were clearly simulated by the DOS method, marking the three sub-states of X, A and B with sticks in Figure 3a. However, the B peak predicted by the DOS method is inconsistent with the experimental spectrum. Our previous study of  $[\text{F}\cdots\text{H}\cdots\text{F}]^-$  anions<sup>67</sup> indicated to us that the spectral complexity can also be derived from vibrational excitations. Using the optimized geometries of the anion and neutral  $\text{H}_2\text{CO}_3\cdot\text{Br}$  complex (Figure 2 and Figure S1), their relative energies, and vibrational frequencies, the predominant FC transitions were calculated and noted with colour sticks in Figure 3b. Apparently, vertical transitions are dominant for the three sub-states due to the similar geometries of both neutral and anion. The FC simulated spectrum is extremely consistent with the experimental spectrum. Encouraged by the good agreement between the FC simulated and experimental spectra, the FC factor calculations were also used to simulate the complicated and distinctive spectrum of  $\text{H}_2\text{CO}_3\cdot\text{F}^-$  in order to clarify its contributors.

Contrary to the relatively simple spectra of other carbonic acid-halide anions, a gently rising edge is observed at the onset region of

the broad band for  $\text{H}_2\text{CO}_3\cdot\text{F}^-$ , covering an eBE range of 4.5–5.5 eV. In addition, large noises blurred the actual spectral signals at the highest eBE region in Figure 2. Thus, the spectral feature at lower eBEs becomes the key criteria to perform FC simulations. It is especially worth noting that in the neutral  $\text{H}_2\text{CO}_3\cdot\text{F}$  complex (Figure S1) two types of hydrogen bonds are clearly identified as  $\text{O}\cdots\text{H}\cdots\text{F}$  and  $\text{O}\cdots\text{H}\cdots\text{F}$ , respectively, in which the fluorine atom acts as both an acceptor and donor of two hydrogen bonds. In contrast, in the anionic state,  $\text{F}^-$  only plays the proton-acceptor role for the double hydrogen bonds in  $\text{H}_2\text{CO}_3\cdot\text{F}^-$ , as shown in Figure 2. Such a dramatic anion  $\rightarrow$  neutral geometry change associated with hydrogen relocation not only results in its extremely small photodetachment cross section per energy interval, but it also produces a large difference between VDE and ADE, as indicated in Table 1. Moreover, extensive vibrational modes are expected to be excited in photodetachment based on this significant geometry rearrangement. Such a complicated spectrum of  $\text{H}_2\text{CO}_3\cdot\text{F}^-$  might be expected from its distinctive delocalized HOMO, implicated in Figure 2.

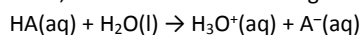
As shown in Figure 3c, the FC simulated spectrum is consistent with the experimental data, especially in the rising edge at lower eBEs. Indeed, massive vibrational transitions are involved and six dominant peaks centered at 5.55, 5.86, 6.25, 6.64, 7.01 and 7.43 eV, respectively, emerge from the simulation, yielding a simulated spectrum that is in overall good agreement with the experimental profile. The two simulated bands at 7.01 and 7.43 eV, however, have much less intensity compared to the experiments, most likely due to other detachment channels kicked in. In addition, for  $\text{H}_2\text{CO}_3\cdot\text{F}^-$ , Isomers 2–4 have a slightly higher energy relative to Isomer 1 by 14.15, 13.62 and 14.00 kJ/mol, respectively. Thus, they could possibly survive from electrospray ionization source and contribute to the experimental spectra, even though their thermal populations based on Boltzmann distribution are only  $\sim 0.5\%$  at 298 K and even less in the low-temperature trap. To rule out their contributions, the FC factor calculations and the spectral simulations were also carried out for these isomers. As shown in Figure S4 and S5, the FC simulated spectra of Isomers 2, 3 and 5 are obviously far different from the experimental data, indicating no contributions from these isomers (an almost  $90^\circ$  rotation of HF around  $\text{HCO}_3$  in the anion  $\rightarrow$  neutral transition causes diminished FCFs for Isomer 4). At this stage, we have identified the structure of all  $\text{H}_2\text{CO}_3\cdot\text{X}^-$  complexes to be dual hydrogen bonded Isomer 1 without PT during complex anion formation based on good agreements between observed and simulated spectra as well as between measured and calculated ADEs and VDEs.

#### How to describe diprotic oxyacid-halide complexes: PA or pKa?

Of special interest is what is the most determinant factor in stabilizing carbonic acid-halide complexes, which is also the key point to unveil different geometries of  $\text{H}_2\text{CO}_3\cdot\text{X}^-$  and  $\text{H}_2\text{SO}_4\cdot\text{X}^-$ .<sup>30</sup> It is well-known that PA plays a pivotal role in determining hydrogen-bonding structures in related complex systems. As a thermodynamic parameter, PA can successfully describe the proton attraction ability of an isolated base in the gas phase, such as in the complex formation between hexafluoroisopropanol (HFIP) and halogen anions  $\text{X}^-$  ( $\text{X} = \text{F}, \text{Cl}, \text{Br}, \text{and I}$ ).<sup>68</sup> We must emphasize that the correlation between the PA of anion and the hydrogen-bonding

strength is true for the system with a single hydrogen bond, e.g. Isomers 2, 3 and 4 (including Isomer 5) of  $\text{H}_2\text{CO}_3 \cdot \text{X}^-$  ( $\text{X} = \text{F}, \text{Cl}, \text{Br}, \text{and I}$ ). However, in a complicated structure like Isomer 1 that involves formation of two hydrogen bonds, the prediction based on purely the PA sequence is incorrect because of no proton-transfer from the carbonic acid moiety to the fluoride anion, as discussed above. A similar phenomenon also existed in the  $\text{H}_2\text{SO}_4 \cdot \text{X}^-$  ( $\text{X} = \text{F}, \text{Cl}, \text{Br}, \text{and I}$ ) system.<sup>30</sup> From the PA perspective, all  $\text{X}^-$  anions could readily attract a proton from sulfuric acid due to their higher PAs than  $\text{HSO}_4^-$ . However, the recent investigation confirmed the opposite conclusions,<sup>30</sup> such that no PT occurs between  $\text{H}_2\text{SO}_4$  and  $\text{X}^-$  ( $\text{X} = \text{Cl}, \text{Br}, \text{and I}$ ), and that the true complex structure is  $[\text{H}_2\text{SO}_4 \cdot \text{X}^-]$  with two  $\text{O}-\text{H} \cdots \text{X}^-$  hydrogen bonds between  $\text{H}_2\text{SO}_4$  and  $\text{X}^-$ . Therefore, PAs of the constituent bases cannot correctly predict the chemistry for proton bound systems that involve the formation of multiple hydrogen bonds.

In contrast, the acid dissociation constant ( $pK_a$ ) has always been used to reflect the ability of acids releasing a proton in aqueous solutions, as shown in the following definition (2):



$$pK_a = -\log_{10}([\text{H}_3\text{O}^+][\text{A}^-]/[\text{HA}]) \quad (2)$$

The competition between the proton acceptors of  $\text{A}^-$  and oxygen atom of water is taken into account in  $pK_a$ , while in the gas phase only one proton attraction of a molecule is included in the PA definition. For a diprotic oxyacid in the *trans-trans* conformation, like Isomer 1 of  $\text{H}_2\text{CO}_3 \cdot \text{X}^-$ , two identical hydroxyls interact with  $\text{X}^-$  simultaneously when approached by anions. This synergistic interaction is evidently different from the isolated attraction elucidated in the PA definition, resulting in its invalidity. Notably, this complicated interaction among two hydroxyls and  $\text{X}^-$  is similar in some extent to the situation of diprotic oxyacid in aqueous solution, in which  $\text{X}^-$  plays the same role as oxygen atom of water. Consequently, the  $pK_a$  might be able to properly predict the occurrence of proton-transfer in the diprotic oxyacid-halide complex anions. Table 2 summarizes the  $pK_a$  values of all acids involved in this work, i.e.  $\text{H}_2\text{CO}_3$ ,  $\text{H}_2\text{SO}_4$ , HF, HCl, HBr and HI, as well as the PA data of the related species,  $\text{HCO}_3^-$ ,  $\text{HSO}_4^-$ ,  $\text{F}^-$ ,  $\text{Cl}^-$ ,  $\text{Br}^-$  and  $\text{I}^-$ .

It is very exciting that a qualitative consistency was captured for these acids in order to explain the perplexing phenomena of proton transfer in their most stable isomers with two hydrogen bonds in accordance to their  $pK_a$  trend. Because the  $pK_a$  values of all HX ( $\text{X} = \text{F}, \text{Cl}, \text{Br}, \text{and I}$ ) acids are smaller (more acidic) than that of  $\text{H}_2\text{CO}_3$  no proton transfer occurs in the formation of Isomer 1 of  $\text{H}_2\text{CO}_3 \cdot \text{X}^-$ . On the contrary, it is feasible to transfer one proton from  $\text{H}_2\text{SO}_4$  hydroxyl to  $\text{F}^-$  due to the lower  $pK_a$  of sulfuric acid, although the proton transfer is not allowed in the other halide anion cases because their  $pK_a$  values are lower than that of  $\text{H}_2\text{SO}_4$ . Therefore, compared with PA,  $pK_a$  can better describe the most stable hydrogen bonding structures of diprotic oxyacid-halide anions.

**Table 2.** The  $pK_a$  values of the acids,  $\text{H}_2\text{CO}_3$ ,  $\text{H}_2\text{SO}_4$  and HX ( $\text{X} = \text{F}, \text{Cl}, \text{Br}, \text{and I}$ ), together with the PAs (in kJ/mol) of the corresponding anions.

	$\text{H}_2\text{CO}_3$	$\text{H}_2\text{SO}_4$	HF	HCl	HBr	HI
$pK_a^a$	6.35	-3.0	3.17	-5.9	-8.8	-9.5
PA <sup>b</sup>	1490	1295	1556	1395	1353	1315

<sup>a</sup>The  $pK_a$  values of  $\text{H}_2\text{CO}_3$ ,  $\text{H}_2\text{SO}_4$  and HF are from Ref. 69, and those of HCl, HBr and HI are from Ref. 70. <sup>b</sup>The corresponding anions are  $\text{HCO}_3^-$ ,  $\text{HSO}_4^-$ ,  $\text{X}^-$  ( $\text{X} = \text{F}, \text{Cl}, \text{Br}, \text{and I}$ ), respectively. The PA value of  $\text{HCO}_3^-$  is from Ref. 56, and the others are from Ref. 55.

Additionally, it is meaningful to assess the BE between acid and halide anions based on their PA values. With the PA decrease along the  $\text{F}^- \rightarrow \text{Cl}^- \rightarrow \text{Br}^- \rightarrow \text{I}^-$  sequence, the BE value of  $\text{H}_2\text{CO}_3 \cdot \text{X}^-$  was reduced monotonically, as mentioned above, owing to the weakened double hydrogen bonding interactions. As a result, the formation of  $\text{H}_2\text{CO}_3 \cdot \text{X}^-$  complex anions is more and more difficult for larger halides. To verify this conclusion, we performed ab initio calculations on Gibbs free energy for formation of Isomer 1  $\text{H}_2\text{CO}_3 \cdot \text{X}^-$  complexes. As listed in Table S3, the  $\Delta_f G_{298.15}$  values increase progressively in the atomic sequence. Notably, the negative  $\Delta_f G_{298.15}$  values were determined for  $\text{H}_2\text{CO}_3 \cdot \text{X}^-$  ( $\text{X} = \text{F}, \text{Cl}, \text{and Br}$ ), but a positive value was obtained for  $\Delta_f G_{298.15}$  of  $\text{H}_2\text{CO}_3 \cdot \text{I}^-$ . Thus, from the thermodynamic perspective,  $\text{H}_2\text{CO}_3 \cdot \text{X}^-$  ( $\text{X} = \text{F} \rightarrow \text{Cl} \rightarrow \text{Br} \rightarrow \text{I}$ ) complex anions are increasingly difficult to generate at room temperature. Fortunately, the exceedingly soft electrospray ionization source, together with the rapid cooling in the cryogenic trap employed in our experiments allowed us to successfully retain these weakly bound species.

## Conclusions

The holistic  $\text{H}_2\text{CO}_3 \cdot \text{X}^-$  ( $\text{X} = \text{F}, \text{Cl}, \text{Br}, \text{and I}$ ) complex anions have been successfully observed in the present experiments, indicative of efficient stabilization of carbonic acid by halide anions. We further carried out a joint experimental and theoretical study on NIPE spectra of  $\text{H}_2\text{CO}_3 \cdot \text{X}^-$ . For the  $\text{X} = \text{Cl}, \text{Br}$  and  $\text{I}$  cases, the observed spectral patterns are similar to the respective  $\text{X}^-$  by shifting to the high electron binding energy side. For  $\text{H}_2\text{CO}_3 \cdot \text{F}^-$ , an extremely wide band was recorded, spanning the eBE range from 4.5 to 7.6 eV. A special six-membered ring structure is suggested for the most stable isomer 1 of  $\text{H}_2\text{CO}_3 \cdot \text{X}^-$ , in which the carbonic acid moiety adopts a planar *trans-trans* conformation. Notably, two identical  $\text{O}-\text{H} \cdots \text{X}$  hydrogen bonds are formed with the approach of  $\text{X}^-$ , which is believed as the key for the formation and stabilization of carbonic acid-halide complexes. Upon electron detachment, only marginal geometry changes are observed for the  $\text{X} = \text{Cl}, \text{Br}, \text{and I}$  complexes. In contrast, significant geometric rearrangement associated with electron-detached hydrogen atom relocation from carbonic acid to fluoride is unravelled, manifested by the appearance of the extraordinary complexity in the  $\text{H}_2\text{CO}_3 \cdot \text{F}^-$  spectrum.

Special attention has been paid to determine the most important factor in stabilizing hydrogen bonding structures of carbonic acid-halide anions. It appears that PA can be generally used to decide the proton location in proton bound systems that involve only one hydrogen bond, but such a prediction cannot convey correct structural binding motif for diprotic oxyacid-halide



complexes, e.g.  $\text{H}_2\text{CO}_3 \cdot \text{X}^-$  and  $\text{H}_2\text{SO}_4 \cdot \text{X}^-$ , where multiple hydrogen bonding interactions exist. To our delight, we found a perfect consistency between the  $pK_a$  trend of acids and their most stable hydrogen bonding structures, strongly suggesting that  $pK_a$  values are a valid parameter to predict proton locations and binding motifs for stabilization of diprotic oxyacids by halide anions.

### Conflicts of interest

There are no conflicts to declare.

### Acknowledgements

This work was supported by U.S. Department of Energy (DOE), Office of Basic Energy Sciences, Division of Chemical Science, Geosciences, and Biosciences, and performed using EMSL, a national scientific user facility sponsored by DOE's Office of Biological and Environmental Research and located at Pacific Northwest National Laboratory, which is operated by Battelle Memorial Institute for the DOE. The theoretical calculations were conducted on the EMSL Cascade Supercomputer. The financial support of the National Natural Science Foundation of China (No. 21873089) and the National Key Research and Development Program of China (No. 2016YFF0200502) are gratefully acknowledged too.

### Notes and references

- 1 A. J. Andersson, F. T. Mackenzie and A. Lerman, *Global Biogeochem. Cycles*, 2006, **20**.
- 2 N. Stolte and D. Pan, *J. Phys. Chem. Lett.*, 2019, **10**, 5135-5141.
- 3 G. Strazzulla, J. R. Brucato, G. Cimino and M. E. Palumbo, *Planet. Space Sci.*, 1996, **44**, 1447-1450.
- 4 W. Hage, K. R. Liedl, A. Hallbrucker and E. Mayer, *Sci.*, 1998, **279**, 1332-1335.
- 5 M. L. Delitsky and A. L. Lane, *J. Geophys. Res.: Planets*, 1998, **103**, 31391-31403.
- 6 I. Kurtz, J. Kraut, V. Ornekian and M. K. Nguyen, *Am. J. Physiol.: Renal Physiol.*, 2008, **294**, F1009-F1031.
- 7 D. Aminov, D. Pines, P. M. Kiefer, S. Daschakraborty, J. T. Hynes and E. Pines, *Proc. Natl. Acad. Sci. U. S. A.*, 2019, **116**, 20837-20843.
- 8 B. Jönsson, G. Karlström, H. Wennerström and B. Roos, *Chem. Phys. Lett.*, 1976, **41**, 317-320.
- 9 S. A. de Marothy, *Int. J. Quantum Chem*, 2013, **113**, 2306-2311.
- 10 S. Ghoshal and M. K. Hazra, *J. Phys. Chem. A*, 2014, **118**, 2385-2392.
- 11 S. Ghoshal and M. K. Hazra, *RSC Adv.*, 2015, **5**, 17623-17635.
- 12 J. K. Terlouw, C. B. Lebrilla and H. Schwarz, *Angew. Chem. Int. Ed. Engl.*, 1987, **26**, 354-355.
- 13 T. Mori, K. Suma, Y. Sumiyoshi and Y. Endo, *J. Chem. Phys.*, 2009, **130**, 204308.
- 14 J. R. Brucato, M. E. Palumbo and G. Strazzulla, *Icarus*, 1997, **125**, 135-144.
- 15 P. Gerakines, M. H. Moore and R. L. Hudson, *Astron. Astrophys.*, 2000, **357**, 793-800.
- 16 W. Zheng and R. I. Kaiser, *Chem. Phys. Lett.*, 2007, **450**, 55-60.
- 17 C. R. Wu, D. Judge, B. M. Cheng, T. S. Yih, C. Lee and W. Ip, *J. Geophys. Res.: Planets*, 2003, **108**.
- 18 M. Garozzo, D. Fulvio, O. Gomis, M. Palumbo and G. Strazzulla, *Sci.*, 2008, **56**, 1300-1308.
- 19 W. Hage, A. Hallbrucker and E. Mayer, *J. Am. Chem. Soc.*, 1993, **115**, 8427-8431.
- 20 M. Moore and R. Khanna, *Spectrochim. Acta, Pt. A: Mol. Spectrosc.*, 1991, **47**, 255-262.
- 21 G. Bucher and W. Sander, *Sci.*, 2014, **346**, 544-545.
- 22 J. Bernard, R. G. Huber, K. R. Liedl, H. Grothe and T. Loerting, *J. Am. Chem. Soc.*, 2013, **135**, 7732-7737.
- 23 K. Winkel, W. Hage, T. Loerting, S. L. Price and E. Mayer, *J. Am. Chem. Soc.*, 2007, **129**, 13863-13871.
- 24 C. Mitterdorfer, J. Bernard, F. Klauser, K. Winkel, I. Kohl, K. R. Liedl, H. Grothe, E. Mayer and T. Loerting, *J. Raman Spectrosc.*, 2012, **43**, 108-115.
- 25 H. P. Reisenauer, J. P. Wagner and P. R. Schreiner, *Angew. Chem. Int. Ed.*, 2014, **53**, 11766-11771.
- 26 K. Adamczyk, M. Premont-Schwarz, D. Pines, E. Pines and E. T. Nibbering, *Sci.*, 2009, **326**, 1690-1694.
- 27 D. A. Thomas, E. Mucha, M. Lettow, G. Meijer, M. Rossi and G. von Helden, *J. Am. Chem. Soc.*, 2019, **141**, 5815-5823.
- 28 P. Ayotte, S. B. Nielsen, G. H. Weddle, M. A. Johnson and S. S. Xantheas, *J. Phys. Chem. A*, 1999, **103**, 10665-10669.
- 29 W. H. Robertson and M. A. Johnson, *Annu. Rev. Phys. Chem.*, 2003, **54**, 173-213.
- 30 G. L. Hou and X. B. Wang, *J. Phys. Chem. Lett.*, 2019, **10**, 6714-6719.
- 31 G. H. Gardenier, J. R. Roscioli and M. A. Johnson, *J. Phys. Chem. A*, 2008, **112**, 12022-12026.
- 32 I. Alata, M. Broquier, C. Dedonder-Lardeux, C. Jouvet, M. Kim, W. Y. Sohn, S.-s. Kim, H. Kang, M. Schuetz, A. Patzer and O. Dopfer, *J. Chem. Phys.*, 2011, **134**, 074307.
- 33 T. C. Cheng, B. Bandyopadhyay, J. D. Mosley and M. A. Duncan, *J. Am. Chem. Soc.*, 2012, **134**, 13046-13055.
- 34 D. Bing, T. Hamashima, C.-W. Tsai, A. Fujii and J.-L. Kuo, *Chem. Phys.*, 2013, **421**, 1-9.
- 35 T. I. Yacovitch, N. Heine, C. Brieger, T. Wende, C. Hock, D. M. Neumark and K. R. Asmis, *J. Chem. Phys.*, 2012, **136**, 241102.
- 36 G.-L. Hou, X.-B. Wang and M. Valiev, *J. Am. Chem. Soc.*, 2017, **139**, 11321-11324.
- 37 Y. X. Zhao, C. C. Arnold and D. M. Neumark, *J. Chem. Soc. Faraday Trans.*, 1993, **89**, 1449-1456.
- 38 D. W. Arnold, S. E. Bradforth, E. H. Kim and D. M. Neumark, *J. Chem. Phys.*, 1995, **102**, 3493-3509.
- 39 E. Garand, T. Wende, D. J. Goebbert, R. Bergmann, G. Meijer, D. M. Neumark and K. R. Asmis, *J. Am. Chem. Soc.*, 2010, **132**, 849-856.
- 40 X. B. Wang and L. S. Wang, *Rev. Sci. Instrum.*, 2008, **79**, 073108.
- 41 R. Krishnan, J. S. Binkley, R. Seeger and J. A. Pople, *J. Chem. Phys.*, 1980, **72**, 650-654.
- 42 R. A. Kendall, T. H. Dunning Jr and R. J. Harrison, *J. Chem. Phys.*, 1992, **96**, 6796-6806.
- 43 K. L. Schuchardt, B. T. Didier, T. Elsethagen, L. Sun, V. Gurumoorathi, J. Chase, J. Li and T. L. Windus, *J. Chem. Inf. Model.*, 2007, **47**, 1045-1052.
- 44 D. Feller, *J. Comput. Chem.*, 1996, **17**, 1571-1586.
- 45 D. G. Fedorov, S. Koseki, M. W. Schmidt and M. S. Gordon, *Int. Rev. Phys. Chem.*, 2003, **22**, 551-592.
- 46 D. G. Fedorov and M. S. Gordon, *J. Chem. Phys.*, 2000, **112**, 5611-5623.
- 47 T. Nakajima and K. Hirao, *J. Chem. Phys.*, 2000, **113**, 7786-7789.
- 48 W. A. De Jong, R. J. Harrison and D. A. Dixon, *J. Chem. Phys.*, 2001, **114**, 48-53.
- 49 P. J. K. H.-J. Werner, F. R. Manby, M. Schütz, P. Celani, G. Knizia, T. Korona, R. Lindh, A. Mitrushenkov, G. Rauhut, T. B. Adler, R. D. Amos, A. Bernhardsson, A. Berning, D. L. Cooper, M. J. O. Deegan, A. J. Dobbyn, F. Eckert, E. Goll, C. Hampel, A.

- Hesselmann, G. Hetzer, T. Hrenar, G. Jansen, C. Köppl, Y. Liu, A. W. Lloyd, R. A. Mata, A. J. May, S. J. McNicholas, W. Meyer, M. E. Mura, A. Nicklass, P. Palmieri, K. Pflüger, R. Pitzer, M. Reiher, T. Shiozaki, H. Stoll, A. J. Stone, R. Tarroni, T. Thorsteinsson, M. Wang, and A. Wolf, *MOLPRO*, version 2015.1, a package of ab initio programs, 2015.
- 50 G.-L. Hou, J. Zhang, M. Valiev and X.-B. Wang, *Phys. Chem. Chem. Phys.*, 2017, **19**, 10676-10684.
- 51 Q. Yuan, X.-T. Kong, G.-L. Hou, L. Jiang and X.-B. Wang, *Faraday Discuss.*, 2019, **217**, 383-395.
- 52 G.-L. Hou, W. Lin, S. Deng, J. Zhang, W.-J. Zheng, F. Paesani and X.-B. Wang, *J. Phys. Chem. Lett.*, 2013, **4**, 779-785.
- 53 M. Cheng, Y. Feng, Y. Du, Q. Zhu, W. Zheng, G. Czako and J. M. Bowman, *J. Chem. Phys.*, 2011, **134**, 191102.
- 54 H. Haberland, *Z. Phys. A: At. Nucl.*, 1982, **307**, 35-39.
- 55 E. P. J. Linstrom and W. J. Mallard, *National Institute of Standards and Technology*, Gaithersburg MD, 20899, <https://doi.org/10.18434/T4D303>, (retrieved March 15, 2020).
- 56 R. R. Squires, *Int. J. Mass Spectrom. Ion Processes*, 1992, **117**, 565-600.
- 57 J. Zhang, B. Zhou, Z.-R. Sun and X.-B. Wang, *Phys. Chem. Chem. Phys.*, 2015, **17**, 3131-3141.
- 58 X. B. Wang and S. S. Xantheas, *J. Phys. Chem. Lett.*, 2011, **2**, 1204-1210.
- 59 H. Wen, G. L. Hou, Y. R. Liu, X. B. Wang and W. Huang, *Phys. Chem. Chem. Phys.*, 2016, **18**, 17470-17482.
- 60 R. F. Bader, *Chem. –A Eur. J.*, 2006, **12**, 7769-7772.
- 61 R. F. Bader and H. Essén, *J. Chem. Phys.*, 1984, **80**, 1943-1960.
- 62 T. Lu and F. Chen, *J. Comput. Chem.*, 2012, **33**, 580-592.
- 63 R. W. Taft, I. Koppel, R. Topsom and F. Anvia, *J. Am. Chem. Soc.*, 1990, **112**, 2047-2052.
- 64 B. N. Plakhutin and E. R. Davidson, *J. Phys. Chem. A*, 2009, **113**, 12386-12395.
- 65 D. J. Tozer and N. C. Handy, *J. Chem. Phys.*, 1998, **109**, 10180-10189.
- 66 V.A. Mozhayskiy and A.I. Krylov, *ezSpectrum*, <http://iopenshell.usc.edu/downloads>.
- 67 G.-L. Hou, X.-B. Wang, A. B. McCoy and W. T. Borden, *J. Phys. Chem. A*, 2017, **121**, 7895-7902.
- 68 L. Wang, Q. Yuan, W. Cao, J. Han, X. Zhou, S. Liu and X.-B. Wang, *J. Phys. Chem. A*, 2020, **124**, 2036-2045.
- 69 Harris, D. C. *Quantitative Chemical Analysis (8th International ed.)*; W. H. Freeman: New York, 2010; p AP12-AP14.
- 70 A. Trummal, L. Lipping, I. Kaljurand, I. A. Koppel and I. Leito, *J. Phys. Chem. A*, 2016, **120**, 3663-3669.